Words count: 7779

# An ANN-based optimization approach of building energy systems: case study of swimming pool

Yantong Li[a,*], Natasa Nord[a], Nan Zhang[b], Cheng Zhou[c]

[a]Department of Energy and Process Engineering, Norwegian University of Science and Technology, Trondheim, Norway

[b]Department of Architecture and Civil Engineering, City University of Hong Kong, Tat Chee Avenue, Kowloon, Hong Kong, China

[c]School of Energy Science and Engineering, Central South University, Changsha, China

**\***The corresponding author; Tele: +47-47743538; Email: yantong.li@ntnu.no

**ABSTRACT**

Reliable models are necessary for optimization of building energy systems. However, artificial neural network (ANN) models developed by measured data is hard to accurately reflect physical characteristics of systems due to uncertainties and unpredicted errors during the measuring process. This study proposes an ANN-based optimization approach. The case study of using the proposed heating system for a typical swimming pool of Hong Kong is depicted to clarify this approach. The ANN model is developed using 1,000 sets of data generated from the established simulation platform. Minimizing thermal uncomfortable ratio, total electricity consumption, and lifecycle cost are regarded as the objectives. The Pareto optimal solutions (POSs) are determined by conducting multi-objective optimization using non-dominated sorting genetic algorithm II. The final optimal solutions are gained from POSs using decision-making approaches. Triple-objective optimization results of the case study indicate that final optimal storage tank volume and air-source heat pumps heating capacity, determined using technique for order of preference by similarity to ideal solution, are 77.4 m$^3$ and 273.6 kW, respectively. The corresponding thermal uncomfortable ratio, total electricity consumption, and lifecycle cost are 1.84%, $1.40 \times 10^{10}$ kJ, and €492,491, respectively. Hence, this study provides a meaningful guideline for the field of ANN-based optimization of building energy systems.

**Keywords:** Artificial neural network; Multi-objective optimization; Building energy systems; Outdoor swimming pool; Heating; Decision-making;

**Nomenclature**

<table>
<tr><td>$q_{rd}$</td><td>radiative heat loss (W)</td></tr>
<tr><td>$q_{rw}$</td><td>heat loss caused by refilling fresh water (W)</td></tr>
</table>

*Abbreviations*

$q_{sr}$    heat acquired from sun (W)

| | | | |
|---|---|---|---|
| ANN | artificial neural network | $T_{ab}$ | ambient temperature (ºC) |
| ASHP | air-source heat pump | $T_{cvr}$ | temperature of cover (ºC) |
| BS | building energy system | $T_m$ | PCM melting temperature (ºC) |
| FOS | final optimal solution | $T_p$ | PCM temperature (ºC) |
| LP | linear programming technique for multidimensional analysis of preferences | $T_{pl}$ | pool water temperature (ºC) |
| NSGA-II | non-dominated sorting genetic algorithm II | $T_{pt}$ | maximum water temperature ASHP offers (ºC) |
| PCM | phase change material | $T_{pw}$ | pool water temperature setpoint (ºC) |
| POS | Pareto optimal solutions | $T_{sl}$ | soil temperature (ºC) |
| PT | PCM storage tank | $T_{sy}$ | sky temperature (ºC) |
| TS | technique for order of preference by similarity to ideal solution | $T_w$ | water temperature (ºC) |
| | | $t$ | moment (-) |
| | | $u_{tp}$ | thermal uncomfortable ratio (%) |
| *Symbols* | | $V_{pl}$ | pool volume (m³) |

| | | | |
|---|---|---|---|
| $A_{cd}$ | heat transfer area for conduction (m$^2$) | $V_{pt}$ | PT volume (m$^3$) |
| $A_{pl}$ | surface area of pool (m$^2$) | $x$ | distance (m) |
| $c_{lc}$ | lifecycle cost (€) | | |
| $c_{ld}$ | PCM liquid specific heat (kJ/(kg·K)) | | |
| $c_p$ | PCM specific heat (kJ/(kg·K)) | *Greek symbols* | |
| $c_{sd}$ | PCM solid specific heat (kJ/(kg·K)) | $\beta_1$ | first coefficient in Eqn. (12) (1/s) |
| $c_w$ | water specific heat (kJ/(kg·K)) | $\beta_2$ | second coefficient in Eqn. (12) (1/s) |
| $E_s$ | maximum daily heat amount during open period (kJ) | $\beta_3$ | third coefficient in Eqn. (12) (1/s) |
| $e_{tu}$ | total electricity consumption (kJ) | $\beta_4$ | fourth coefficient in Eqn. (12) (1/s) |
| $H_m$ | PCM specific enthalpy (kJ/kg) | $\varepsilon$ | water fraction (-) |
| $H_p$ | PCM enthalpy (kJ/kg) | $\emptyset_1$ | a constant in Eqn. (18) (°C/s) |
| $h_{cv}$ | heat transfer coefficient for convection (W/(m$^2$·K)) | $\emptyset_2$ | a constant in Eqn. (23) (°C/s) |
| $h_{cvr}$ | heat transfer coefficient for conduction (W/(m$^2$·K)) | $\emptyset_3$ | a constant in Eqn. (20) (°C/s) |
| $h_{rd}$ | radiative heat transfer coefficient (W/(m$^2$·K)) | $\rho_p$ | PCM density (kg/m$^3$) |
| $h_{wp}$ | volumetric heat transfer coefficient (W/(m$^3$·K)) | $\rho_w$ | water density (kg/m$^3$) |

| | | | |
|---|---|---|---|
| $k_{sl}$ | soil thermal conductivity (W/(m·K)) | $\theta_1$ | a constant in Eqn. (17) (°C/s) |
| $k_w$ | water thermal conductivity (W/(m·K)) | $\theta_2$ | a constant in Eqn. (22) (°C/s) |
| $L_{cd}$ | pool characteristic length (m) | $\theta_3$ | a constant for calculating $\emptyset_3$ (°C/s) |
| $m_p$ | PCM mass (kg) | $\tau$ | time (s) |
| $m_w$ | water mass (kg) | $\gamma_1$ | first coefficient in Eqn. (10) (-) |
| $q_{ap}$ | ASHPs heating capacity (W) | $\gamma_2$ | second coefficient in Eqn. (10) (-) |
| $q_{cd}$ | conductive heat loss (W) | $\gamma_3$ | third coefficient in Eqn. (10) (-) |
| $q_{ch}$ | $q_{ap}$ for charging (W) | $u_w$ | average water velocity (m/s) |
| $q_{cv}$ | convective heat loss (W) | $\varphi_1$ | length of the period ($t_0 \rightarrow t_3$) (s) |
| $q_{cvr}$ | heat loss from cover (W) | $\varphi_2$ | length of the period ($t_3 \rightarrow t_4$) (s) |
| $q_{dc}$ | dimensionless conductive heat flux (-) | $\varphi_3$ | length of the period ($t_4 \rightarrow t_5$) (s) |
| $q_{ea}$ | evaporative heat loss (W) | $\Delta_{lw}$ | lower temperature difference (K) |
| $q_{pr}$ | $q_{ap}$ for preheating (W) | $\Delta_{uw}$ | upper temperature difference (K) |
| $q_{pt}$ | heat acquired from PT (W) | | |

## 1. Introduction

Due to rapid increase of population, demand of energy for satisfying a variety of requirements in life (e.g. transportation, manufacturing, and farming), is continually increasing (Moussa et al., 2020). This causes severe energy crisis, leading to increasing utilization of fossil fuels and environmental problems (e.g. global warming) (Du et al., 2020; 2018). Thus, enhancing renewable energy utilization and energy efficiency, and reducing greenhouse gas emission have gained attentions from governments in different countries. For instance, Chinese government declares that energy use in each unit of GDP will be reduced by 15% during the period of next five years (Kennedy and Johnson, 2016). EU government declares that energy efficiency will be increased by more than 32.5% by 2030 (Abd Alla et al., 2020). In addition, South Korean government declares that 12.2% energy use will be from renewable energy source by 2030 (Sinha et al., 2018).

Cities consume at least 67% of the world's total energy use (Fichera et al., 2018). To enhance cities' energy efficiency, scholars have conducted different investigations of urban energy systems. For example, Volpe et al. (2016) investigated the effect of energy systems on the energy networks performance in cities, and they found that the increase of the radius of proximity could enhance the performance of urban energy networks. Evola et al. (2016) proposed a mapping tool used in a neighborhood of Catania, Italy. It was concluded that this tool could effectively offer polices with high energy-saving potential. In addition, buildings consume 31% (Schwarz et al., 2020) to 42% (Mavromatidis, 2015; 2016) of the world's gross energy use and emit 35% of the world's gross greenhouse gas (Mavromatidis, 2015; 2016). Hence, advanced approaches are urgently needed for enhancing energy efficiency and reducing greenhouse gas emission of building energy systems (BSs). One efficient approach is to perform the optimal design of BSs. For instance, Li et al. (2019) presented the optimization of photovoltaic shading systems. The optimal installation tilt angle was determined for gaining better energy-saving potential. Liu et al. (2019) presented the optimization of a photovoltaic zero-energy building system. The system performance in different locations of China were compared, and it was discovered that southwest regions in China was the optimal site to achieve the best energy performance. Gang et al. (2016) performed the optimization of district cooling systems. Minimizing total expense by determining optimal cooling capacity of the system was considered as optimization objective.

Artificial neural network (ANN) is a data-driven tool that develops surrogated models with high accuracy (von Grabe, 2016), and it has been extensively used in BSs. For instance, Turhan et al. (2014) applied the ANN for predicting relationships between the heating load and configuration parameters of buildings (e.g. external surface area). The data collected from 148 residential buildings in Izmir, Turkey, were used. Deng and Chen (2018) utilized the ANN for establishing the thermal comfort model in buildings, on the basis of data collected from ten houses or apartments and ten offices in Indiana, USA. The relationships between thermal comfort and affecting parameters (e.g. indoor temperature) were predicted. In addition, using the data collected from an office building with the floor area of 5,700 $m^2$, Ding et al. (2018) compared the performance of the established ANN models in eight combinations of input variables (e.g. solar irradiance and ambient temperature), and the optimal combination was identified. Current studies (e.g. above-mentioned studies) focused on the development of ANN models directly based on the measured or field data. However, the measured or field data cannot well reflect physical characteristics of investigated BSs due to uncertainties and unpredicted errors.

As described in the study of Bejan (2015), physical characteristics are important for investigated systems including BSs. Recently, based on the "construal law", Mavromatidis (2019) developed an urban greenhouse model, which considers thermodynamic properties of buildings (e.g. convective and radiative heat fluxes). It was concluded that the method used by this author effectively combined the aspects of "physics" and "sustainability" in the field of architecture, which played the instructive role in future optimal design problems of BSs (Mavromatidis, 2018). Hence, it is meaningful to consider physical characteristics during the investigation process of BSs, especially developing ANN models of BSs.

Optimal design problems are usually based on only one optimization objective. However, practical engineering problems should consider multiple aspects, meaning that multiple optimization objectives should be used in optimal design problems. Hence, multi-objective optimization of many systems is widely conducted. For instance, Zhou and Zeng (2020) presented the multi-objective optimization of an aerogel glazing system. Maximizing indoor illuminance transmitted and minimizing indoor heat harvest were regarded as optimization objectives. Ya et al. (2019) presented the multi-objective optimization of the power system combining cooling, heating, and power. The optimization objectives comprised minimizing

total cost and size of the system. Tang and Zhang (2019) conducted the multi-objective optimization of the combustion systems, where minimizing $NO_x$ emission and maximizing combustion efficiency were regarded as the objectives. Chen et al. (2018) presented the multi-objective optimization of a desalination system with the objectives of minimizing initial cost, greenhouse gas emission, and energy use. Although multi-objective optimal design has been conducted in a few systems, a systematic and comprehensive multi-objective optimal design method based on high-accuracy surrogated models (e.g. ANN models) is still lacking. It should be noted that although some scholars have conducted the optimal design combining the ANN and optimization algorithm (e.g. Nasruddin et al. (2019)), a general method that can be used to well guide engineers and researchers to conduct the optimal design is urgently needed.

Recently, designing superior heating systems for outdoor swimming pools is still a research hotspot. Outdoor swimming pool is closed in cold seasons in subtropical climates, since weather conditions cannot provide enough thermal energy to satisfy thermal comfort requirement (Li et al., 2018b). The energy use is very high when traditional heating systems (e.g. electric or gas boilers) are applied to extend the availability of pools (Mousia and Dimoudi, 2015). Thus, advanced heating systems are proposed to deal with this issue. One popular system is to use solar collectors. Dang (1986) utilized solar collectors to offer heat to a swimming pool in India. The system energy efficiency was reported to be 53.3%. Another popular system is to utilize heat pumps. Lam and Chan (2003; 2001) utilized air-source heat pumps (ASHPs) for warming a swimming pool with the volume of 52 $m^3$. It was discovered that ten-year energy cost of the proposed system was decreased by HK$275,700 (i.e. approximately €33,084, note: HK$1 = €0.12) in comparison with that of the conventional system. Following their studies, Li et al. (2018a) designed a system with a tank having phase change material (PCM) (i.e. PCM storage tank (PT)), which had merit of high storage density (Xu et al., 2017; 2018). The PT was applied to shift the energy consumption of ASHPs from electric on-peak to off-peak periods. This could cut down not only system operating cost, but also designed ASHPs heating capacity ($q_{ap}$). Although a few studies have presented the investigations of swimming pool heating systems, an efficient optimization approach, especially an ANN-based multi-objective optimization approach for swimming pool heating applications, is needed.

This study puts forward an ANN-based multi-objective optimization approach of BSs. As a

typical BS, outdoor swimming pool heating system is regarded as a case study to clarify the proposed approach. Database of the system is developed, based on huge amount of operation results from established simulation platform. ANN is utilized to establish the system model. The non-dominated sorting genetic algorithm II (NSGA-II) (Deb et al., 2002) is applied for performing the multi-objective optimization. Linear programming technique for multidimensional analysis of preferences (LP) (Srinivasan and Shocker, 1973) and technique for order of preference by similarity to ideal solution (TS) (Etghani et al., 2013) are applied to conduct the decision-making for determining final optimal solutions (FOSs). Finally, the system performance analysis of FOSs is presented.

The novelties or contributions of this investigation are depicted below: (a) development of a general optimal design method combining the use of ANN model and NSGA-II, and its application to an outdoor swimming pool heating system; (b) development of the ANN model based on a database composed by 1,000 sets of data, generated by the established simulation platform using MATLAB and TRNSYS; (c) use of NSGA-II for multi-objective optimizations to determines the POSs; (d) implementation of LP and TS on the POSs to effectively determine the FOSs; (e) demonstration of the reliability of proposed approach on the basis of a case study of an outdoor swimming pool heating system.

The rest of the paper is presented below. The proposed ANN-based multi-objective optimal design method is presented in Section 2. The case study is described in Section 3. The ANN model is given in Section 4. The establishment of database is shown in Section 5. Section 6 introduces optimization and decision-making methods. Section 7 shows the results and analysis. Section 8 depicts conclusions.

## 2. ANN-based multi-objective optimization approach

Fig. 1 presents the schematic for proposed ANN-based multi-objective optimization approach of BSs consisting of five steps. ***Step 1 is conducting the database construction.*** According to the characteristics of investigated systems, the maximum and minimum of design variables should be identified. Ranges of design variables are used to formulate combinations of design variables. These combinations are input into constructed simulation platform of the system, which generally comprises heat transfer models, weather conditions, and control strategies. The corresponding values of output variables are acquired for each combination of design

8

variables. Thus, the database of input and output variables is constructed. ***Step 2 is conducting the ANN training.*** On the basis of constructed database, input, hidden, and output layers of ANN structure are established. The training algorithm and parameters are set for training the ANN. Training, testing, and validation performance of different ANN structures are compared, and the optimal structure is determined. Consequently, the validated ANN models are obtained. ***Step 3 is conducting the multi-objective optimal design.*** ANN models and identified multiple optimization objectives are used to conduct the multi-objective optimal design by advanced algorithm. The POSs are gained. ***Step 4 is conducting the decision-making.*** Quantitative approaches are utilized to perform the decision-making for obtaining FOSs. ***Step 5 is conducting the performance analysis.*** System performance analysis for FOSs are conducted by using typical performance indicators.
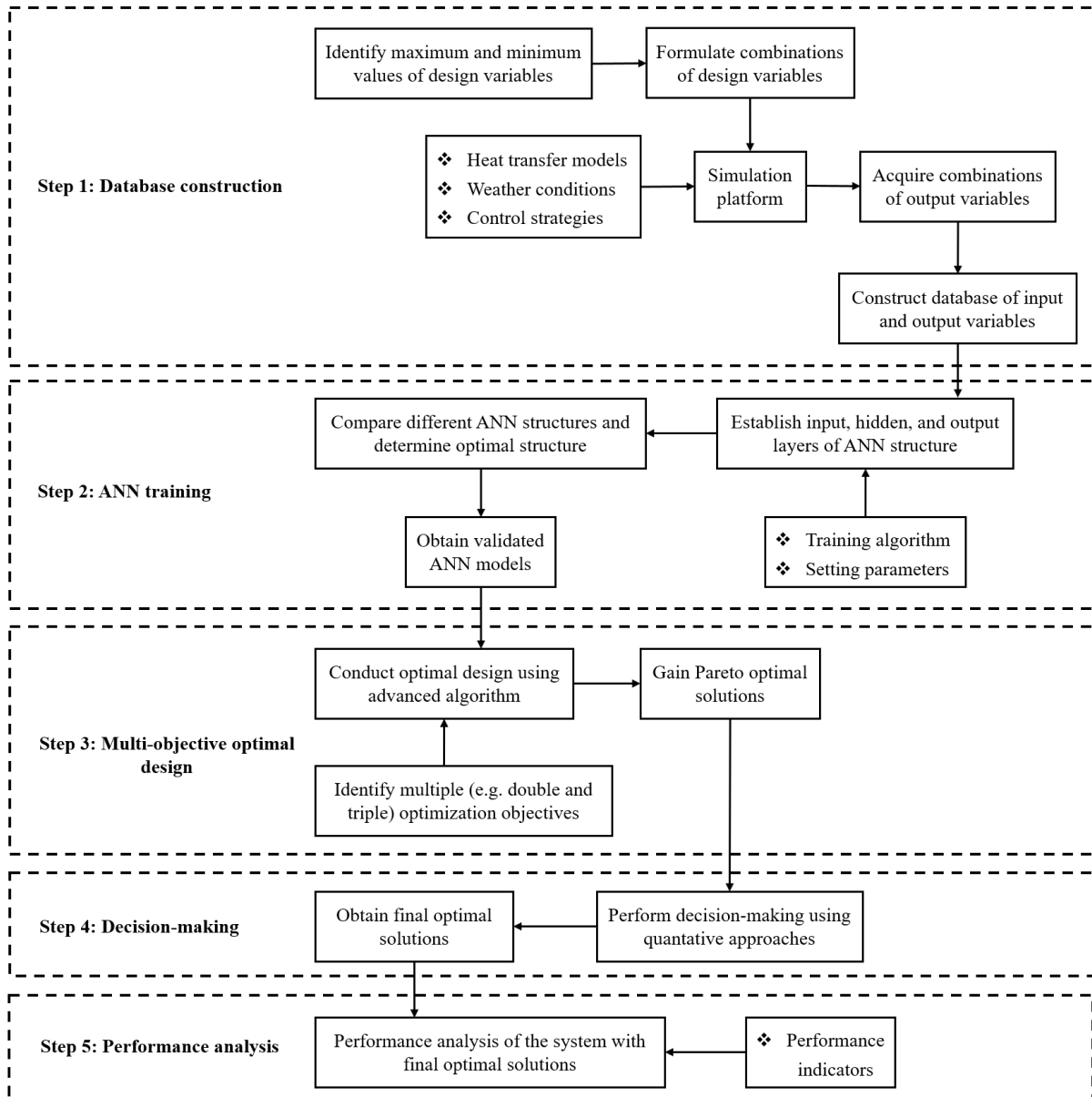
**Fig. 1.** Schematic of ANN-based multi-objective optimization approach.

## 3. Case study

Fig. 2 (a) presents the schematic of a heating system for outdoor swimming pools, which includes PT, ASHPs, insulation cover, heat exchangers, pumps, valves, etc. ASHPs are utilized to realize charging of PT and preheating of the pool water. PT stores heat in electric off-peak period and releases stored heat in electric on-peak period. This contributes to enhancing economic benefits. Insulation cover is covered in pool surface when it is not used. This contributes to preventing heat loss. It should be noted that this system can be used for space heating purpose as well. In that case, the outdoor swimming pool will be replaced by radiators,

10

which heat the air of the room. The control strategies depicted in the study of Li et al. (2020a) are used to achieve the desired temperature profile of the pool water, depicted in Fig. 2 (b).
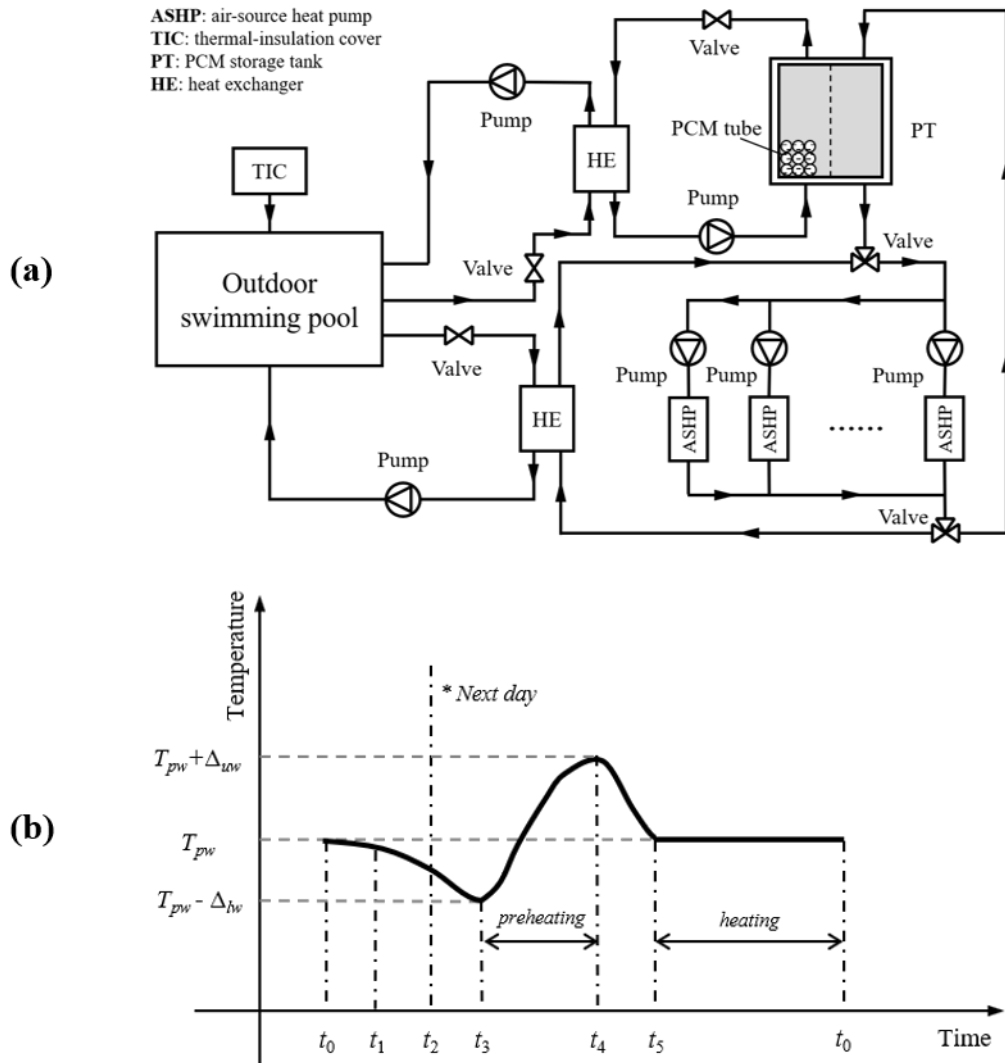


**Fig. 2.** (a) Schematic of the system; and (b) pool water temperature profile.

The system is applied in an outdoor swimming pool of Hong Kong. Its volume and surface area are 1963.5 m³ and 1100 m², respectively. It is closed during the cold season on account of the cold weather. This leads to space and facility waste. Therefore, the system is applied for extending the availability of the pool. The values of corresponding moments in Fig. 2 (b) are shown as follows. $t_0$, $t_1, t_2, t_3, t_4$, and $t_5$ are 20:00, 21:00, 24:00, 05:00, 09:00, and 12:00, respectively.

## 4. Artificial neural network model

In the established ANN model, two design variables (i.e. Volume of PT ($V_{pt}$) and $q_{ap}$) are selected as input variables. Thermal uncomfortable ratio ($u_{tp}$), total electricity consumption ($e_{tu}$), and lifecycle cost ($c_{lc}$) are selected as output variables. The schematic of ANN structure is depicted in Fig. 3 (a). The definitions for these three output variables are depicted in the study of Li et al. (2020b), and information about unit expenses of core components are shown in the study of Li et al. (2020a). A feedforward neural network with the training function of "trainlm", which uses the Levenberg-Marquardt algorithm, is used in this study. The values of maximum number of training epochs, maximum mu, performance goal, and maximum validation failures are 5,000, $1\times10^{100}$, $1\times10^{-10}$, and 3,000, respectively. The values of other parameters are default. 70%, 15%, and 15% of the data are selected for the training, testing, and validation purpose, respectively. The selection for data is random. An early-stopping principle is used to identify the optimal epoch for identifying the trained model. The epoch is considered as optimal one when the validation error achieves minimum. As depicted in Fig. 3 (b), during training process, the training error reduces with the increase of the epoch; while the validation error firstly reduces with the increase of the epoch, and then increases as the epoch increases.
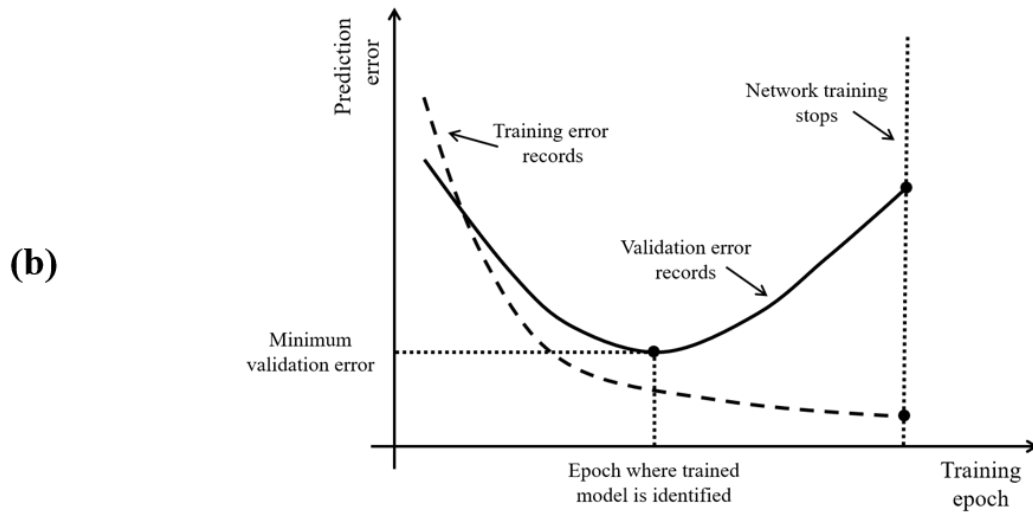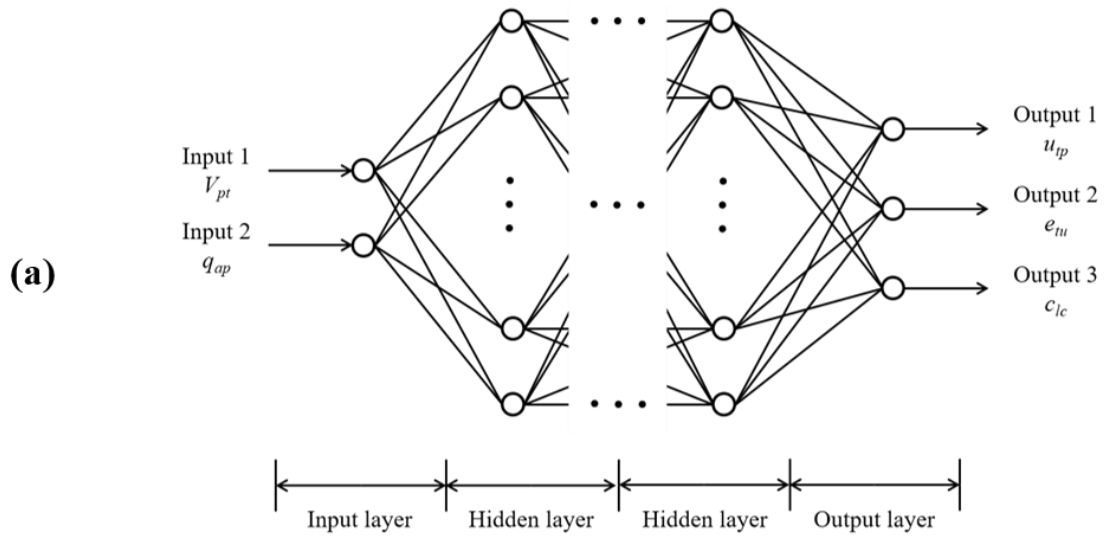
**Fig. 3.** (a) Schematic for ANN structure; and (b) early-stopping principle for training ANN model.

## 5. Database establishment

One hundred design cases (i.e. combinations of design variables) are performed in accordance with maximum and minimum sizing of core components. They are input into established simulation platform of the system to obtain corresponding output values. Ten-winter Hong Kong weather data (from 2003 to 2012) are used in these design cases. Hence, 1,000 sets of data are utilized to establish the database for the ANN model.

5.1. Maximum sizing for core components

The proposed maximum sizing approach of core components of the system is shown in Fig. 4, which utilizes three factors (i.e. worst-case scenario, weather conditions, and pool water temperature setpoint ($T_{pw}$)). The weather conditions that significantly influence the heat transfer process are essential requirement during sizing process. The worst-case scenario is utilized to identify the meteorological condition that causes the maximum heat loss of pool. $T_{pw}$ is an important design variable that directly affects the required heat amount. Heat transfer model of pool without cover is applied to calculate maximum daily heat amount during the open period ($t_5 \rightarrow t_0$) ($E_s$). According to this value, the $V_{pt}$ and required $q_{ap}$ for charging ($q_{ch}$) are calculated by using Eqns. (3) and (25), respectively. Heat transfer model of pool with cover is utilized to calculate the temperature difference $\Delta_{uw}$ and $\Delta_{lw}$ shown in Fig. 5, by using Eqns. (20) and (19), respectively. These two values are used to calculate the required $q_{ap}$ for preheating ($q_{pr}$) by using Eqn. (24). The final required $q_{ap}$ should satisfy two goals (i.e. ensuring the completion of preheating and charging). Thus, the maximum between $q_{ch}$ and $q_{pr}$ is estimated as the final $q_{ap}$. The detailed calculations during the maximum sizing process are presented as follows.
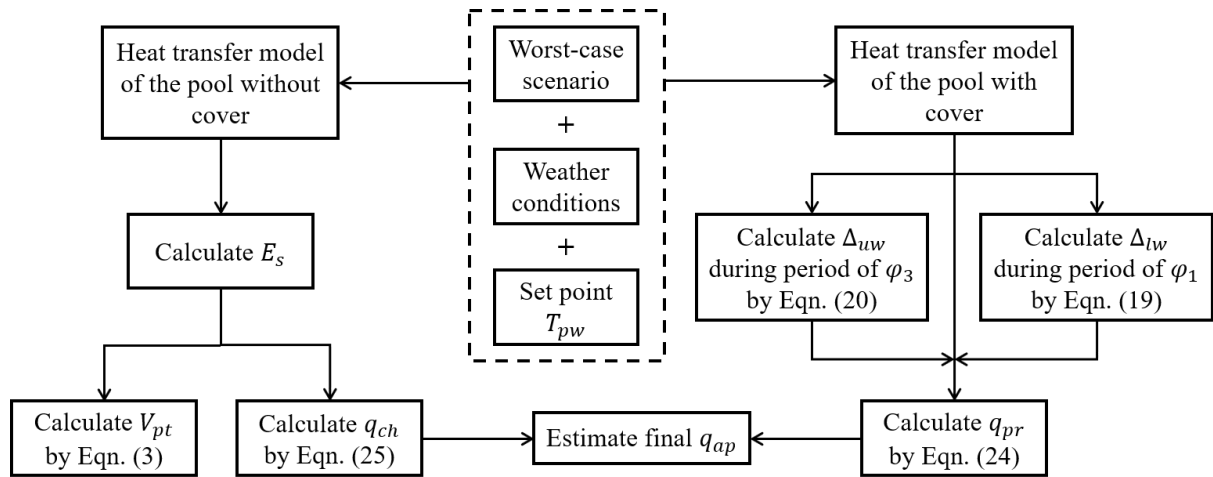


**Fig. 4.** Maximum sizing approach of core components.

● **Calculation of $V_{pt}$**

Heat transfer model of pool without cover is applied for calculating the $E_s$. The pool water temperature variation is expressed as Eqn. (1) (Buonomano et al., 2015; Somwanshi et al.,

2013):

$$\rho_w c_w V_{pl} \frac{dT_{pl}}{d\tau} = q_{sr} - q_{ea} - q_{rd} - q_{cv} - q_{cd} - q_{rw} \tag{1}$$

where $\rho_w$ and $c_w$ are the water density and specific heat, respectively; $V_{pl}$ is the pool volume; $T_{pl}$ is the pool water temperature; $\tau$ is the time; $q_{sr}$ is the heat acquired from sun; and $q_{ea}$, $q_{rw}$, $q_{cv}$, $q_{cd}$, and $q_{rd}$ are the evaporative, refilling water, convective, conductive, and radiative heat loss, respectively. Equations for calculating $q_{sr}$, $q_{ea}$, $q_{rw}$, $q_{cv}$, $q_{cd}$, and $q_{rd}$ refer to the study of Lam and Chan (2001), Smith et al. (Buonomano et al., 2015; Ruiz and Martínez, 2010), Lam and Chan (2001), Buonomano et al. (2015), Incropera et al. (2007), and Woolley et al. (2011), respectively.

$E_s$ should be equal to the heat amount stored in PT, which is calculated by the difference between $T_{pw}$ and $T_{pt}$, expressed as Eqn. (2):

$$E_s = \left(c_p m_p + c_w m_w\right)\left(T_{pt} - T_{pw}\right) + m_p H_m \tag{2}$$

where $m_w$ represents the water mass; $c_p$ and $m_p$ represent the PCM specific heat and mass, respectively; and $H_m$ represents the PCM specific enthalpy. Considering thermal properties of PCM, Eqn. (2) is reformulated as Eqn. (3):

$$V_{pt} = \frac{E_s}{c_{ld}\rho_p(1-\varepsilon)(T_{pt}-T_m)+H_m\rho_p(1-\varepsilon)+c_{sd}\rho_p(1-\varepsilon)(T_m-T_{pw})+c_w\rho_w\varepsilon(T_{pt}-T_{pw})} \tag{3}$$

where $c_{ld}$ and $c_{sd}$ represent the PCM liquid and solid specific heat, respectively; $T_m$ represents the PCM melting temperature; $\rho_p$ represents the PCM density; and $\varepsilon$ represents the water fraction.

The design goal for $\Delta_{uw}$ and $\Delta_{lw}$ is to ensure that the $T_{pl}$ can reach to $T_{pw}$ at $t_5$. To facilitate the calculation, $\varphi_1$, $\varphi_2$, and $\varphi_3$ are utilized to represent the length of the periods $(t_0 \rightarrow t_3)$, $(t_3 \rightarrow t_4)$, and $(t_4 \rightarrow t_5)$, respectively, as depicted in Fig. 5 (a). Fig. 5 (b) depicts the heat fluxes in heat transfer model with cover during the close period $(t_0 \rightarrow t_5)$. It should be noted that the influence of the solar irradiation on the temperature of the cover $(T_{cvr})$ is not considered.
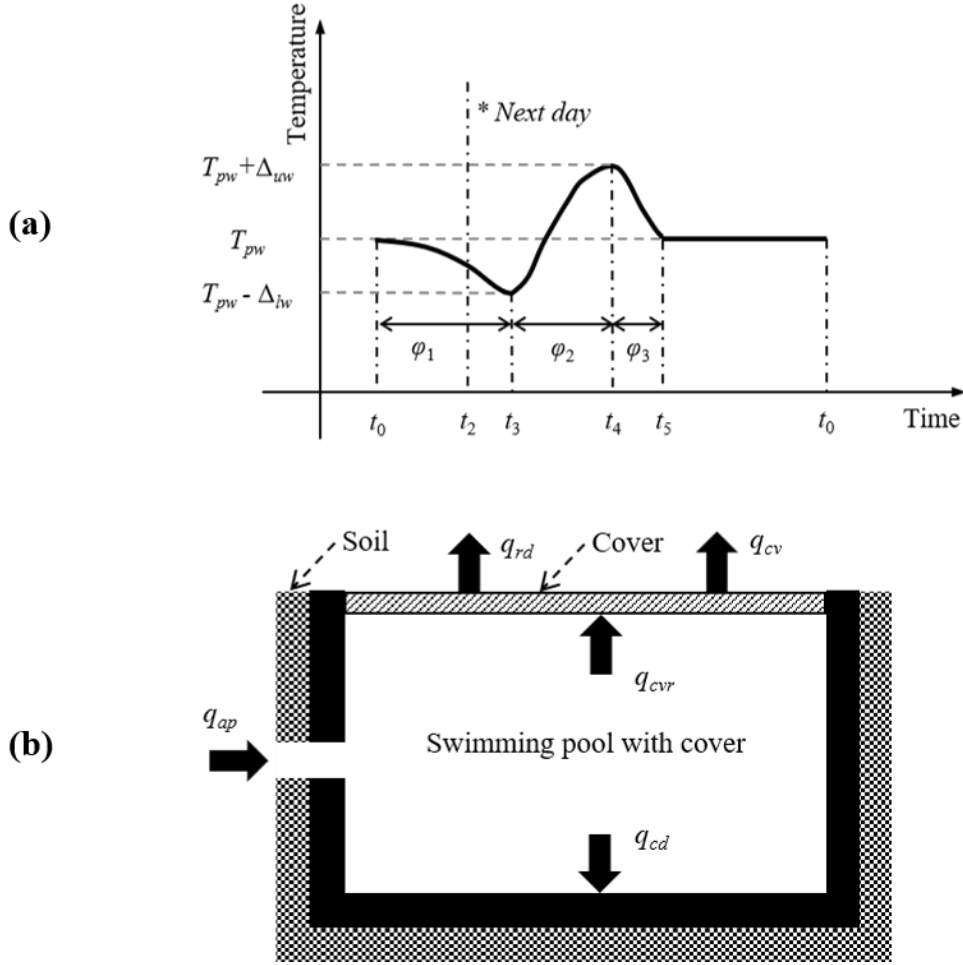
15

**Fig. 5.** (a) Partition of $\varphi_1$, $\varphi_2$, and $\varphi_3$; and (b) heat fluxes during the period ($t_0 \to t_5$).

- **Calculation of $\Delta_{lw}$**

During the period ($t_0 \to t_3$), $T_{pl}$ should satisfy Eqn. (4):

$$\rho_w c_w V_{pl} \frac{dT_{pl}}{d\tau} = -q_{cvr} - q_{cd} \tag{4}$$

where $q_{cvr}$ is the heat loss from the cover.

$q_{cd}$ is calculated by Eqn. (5) (Incropera et al., 2007):

$$q_{cd} = \frac{1}{2L_{cd}} q_{dc} k_{sl} A_{cd} (T_{pl} - T_{sl}) \tag{5}$$

where $L_{cd}$ denotes the pool characteristic length; $q_{dc}$ denotes the dimensionless conductive heat flux; $k_{sl}$ denotes the soil thermal conductivity, equal to 0.52 W/(m·K) (Incropera et al., 2007); $A_{cd}$ denotes the heat transfer area for conduction; and $T_{sl}$ denotes the soil temperature.

16

$q_{cvr}$ is equal to the sum of $q_{rd}$ and $q_{cv}$, expressed as Eqn. (6):

$$q_{cvr} = q_{rd} + q_{cv} \tag{6}$$

$q_{cvr}$ is calculated by Eqn. (7):

$$q_{cvr} = h_{cvr}A_{pl}(T_{pl} - T_{cvr}) \tag{7}$$

$q_{rd}$ is calculated by Eqn. (8):

$$q_{rd} = h_{rd}A_{pl}(T_{cvr} - T_{sy}) \tag{8}$$

where $T_{sy}$ is the sky temperature.

$q_{cv}$ is calculated by Eqn. (9):

$$q_{cv} = h_{cv}A_{pl}(T_{cvr} - T_{ab}) \tag{9}$$

where $T_{ab}$ is the ambient temperature.

According to Eqns. (6) to (9), $T_{cvr}$ is calculated by Eqn. (10):

$$T_{cvr} = \gamma_1 T_{pl} + \gamma_2 T_{sy} + \gamma_3 T_{ab} \tag{10}$$

where

$$\gamma_1 = \frac{h_{cvr}}{h_{cvr}+h_{rd}+h_{cv}}, \ \gamma_2 = \frac{h_{rd}}{h_{cvr}+h_{rd}+h_{cv}}, \ \gamma_3 = \frac{h_{cv}}{h_{cvr}+h_{rd}+h_{cv}} \tag{11}$$

According to Eqns. (5) and (6), Eqn. (4) is reformulated as Eqn. (12):

$$\frac{dT_{pl}}{d\tau} = \beta_1 T_{pl} + \beta_2 T_{sy} + \beta_3 T_{ab} + \beta_4 T_{sl} \tag{12}$$

where the coefficients $\beta_1$, $\beta_2$, $\beta_3$, and $\beta_4$ are calculated by Eqns. (13), (14), (15), and (16), respectively:

$$\beta_1 = -\left[h_{cvr}A_{pl}(1 - \gamma_1) + \frac{1}{2L_{cd}}q_{dc}k_{sl}A_{cd}\right]/(\rho_w c_w V_{pl}) \tag{13}$$

$$\beta_2 = \frac{h_{cvr}A_{pl}\gamma_2}{\rho_w c_w V_{pl}} \tag{14}$$

$$\beta_3 = \frac{h_{cvr}A_{pl}\gamma_3}{\rho_w c_w V_{pl}} \tag{15}$$

$$\beta_4 = \frac{1}{2\rho_w c_w V_{pl}L_{cd}}q_{dc}k_{sl}A_{cd} \tag{16}$$

Assuming that $T_{sy}$, $T_{ab}$, and $T_{sl}$ are constants during this period, Eqn. (12) is reformulated as Eqn. (17):

$$\frac{dT_{pl}}{d\tau} = \beta_1 T_{pl} + \theta_1 \tag{17}$$

where $\theta_1 = \beta_2 T_{sy} + \beta_3 T_{ab} + \beta_4 T_{sl}$. Hence, $T_{pl}$ at the time $t$ is calculated by Eqn. (18):

$$T_{pl}(t) = \frac{\emptyset_1}{\beta_1} e^{\beta_1 t} - \frac{\theta_1}{\beta_1} \tag{18}$$

where $\emptyset_1$ is a constant. At the beginning of this period ($t = 0$), $T_{pl}(0) = T_{pw}$; and at the end of this period ($t = \varphi_1$), $T_{pl}(\varphi_1) = T_{pw} - \Delta_{lw}$. Hence, $\Delta_{lw}$ is calculated by Eqn. (19):

$$\Delta_{lw} = \frac{\emptyset_1}{\alpha_1}\left(1 - e^{\beta_1 \varphi_1}\right) \tag{19}$$

where $\emptyset_1 = \beta_1 T_{pw} + \theta_1$.


- **Calculation of $\Delta_{uw}$**

During the period ($t_4 \rightarrow t_5$), the $T_{pl}$ should also satisfy Eqn. (4). Thus, the solution during this period is expressed as the same format with Eqn. (18). At the beginning of this period ($t = 0$), $T_{pl}(0) = T_{pw} + \Delta_{uw}$, and at the end of this period ($t = \varphi_3$), $T_{pl}(\varphi_3) = T_{pw}$. Hence, $\Delta_{uw}$ is calculated by Eqn. (20):

$$\Delta_{uw} = \frac{\emptyset_3}{\beta_1}\left(1 - e^{\beta_1 \varphi_3}\right) \tag{20}$$

where $\emptyset_3 = (\beta_1 T_{st} + \theta_3)e^{-\beta_1 \varphi_3}$.


- **Calculation of $q_{pr}$**

During the period ($t_3 \rightarrow t_4$), $T_{pl}$ should satisfy Eqn. (21):

$$\rho_w c_w V_{pl} \frac{dT_{pl}}{d\tau} = q_{pr} - q_{cvr} - q_{cd} \tag{21}$$

$q_{pr}$ is a constant during the preheating period, and thus Eqn. (21) is reformulated as Eqn. (22):

$$\frac{dT_{pl}}{d\tau} = \beta_1 T_{pl} + \theta_2 + \frac{q_{pr}}{\rho_w c_w V_{pl}} \tag{22}$$

The solution of Eqn. (22) is expressed as Eqn. (23):

$$T_{pl}(t) = \frac{\emptyset_2}{\beta_1} e^{\beta_1 t} - \frac{\theta_2}{\beta_1} - \frac{q_{pr}}{\beta_1 \rho_w c_w V_{pl}} \tag{23}$$

At the beginning of this period ($t = 0$), $T_{pl}(0) = T_{pw} - \Delta_{lw}$, and at the end of this period

18

$(t = \varphi_2)$, $T_{pl}(\varphi_2) = T_{pw} + \Delta_{uw}$. Thus, $q_{pr}$ is calculated by Eqn. (24):

$$q_{pr} = \frac{\rho_w c_w V_{pl}\left[(\beta_1 T_{pw} - \beta_1 \Delta_{lw} + \theta_2)e^{\beta_1 \varphi_2} - (\beta_1 T_{pw} + \beta_1 \Delta_{uw} + \theta_2)\right]}{1 - e^{\beta_1 \varphi_2}} \tag{24}$$

- **Calculation of $q_{ch}$**

$q_{ch}$ is calculated by Eqn. (25):

$$q_{ch} = \frac{E_s}{(t_3 - t_1)} \tag{25}$$

5.2. Minimum sizing of core components

The minimum values of $V_{pt}$ and $q_{ap}$ are identified in accordance with 10% of maximum heating demands. According to calculations in Section 5.1, the maximum values of $V_{pt}$ and $q_{ap}$ are 278 m³ and 601.7 kW, respectively; while the minimum values of $V_{pt}$ and $q_{ap}$ are 27.8 m³ and 60.2 kW, respectively.

5.3. Constructed simulation platform

The simulation platform is constructed by MATLAB and TRNSYS. The TRNSYS 17 is applied for providing the simulation environment for operation of the system (Klein et al., 2011). Type 647, 649, 3b, 23, 91, and 941 in TRNSYS are utilized to simulate the diverting valves, mixing valves, circulation pumps, PID controllers, heat exchangers, and ASHPs, respectively. The PID controller is applied to maintain the water temperature within thermal comfortable scope. The trial & error method is used to tune the values of gain constant, integral time, and derivative time (TrialandErrorMethod, 2020). In this study, the values of gain constant, integral time, and derivative time are 0.5, 5, and 0, respectively. The time step for the simulation process is 5 minutes. The MATLAB is applied to solve and code swimming pool and PT models. They are linked into the TRNSYS by Type 155. The models of pool with and without cover are presented in Section 5.1. It should be noted that during the open period $(t_5 \rightarrow t_0)$, the heat acquired from the PT $(q_{pt})$ should be added in right-hand side of Eqn. (1).

PT model is established based on several assumptions: (1) no internal heat source exists inside PCM tubes; (2) no heat exchanges between PT and ambient; (3) temperature of water and PCM

19

cannot affect their thermal properties; (4) $T_p$ is constant during the phase change process; (5) temperature only varies along water-flow direction. The governing equation for water side is expressed as Eqn. (26):

$$\rho_w c_w \varepsilon \left(\frac{\partial T_w}{\partial \tau} + u_w \frac{\partial T_w}{\partial x}\right) = k_w \varepsilon \frac{\partial^2 T_w}{\partial^2 x} + h_{wp}(T_p - T_w) \tag{26}$$

where $u_w$ represents the average water velocity; $k_w$ represents the water thermal conductivity; and $x$ represents the distance. The governing equation for PCM side is expressed as Eqn. (27):

$$\rho_p (1 - \varepsilon) \frac{\partial H_p}{\partial \tau} = h_{wp}(T_w - T_p) \tag{27}$$

Eqns. (26) and (27) are discretized using finite difference method (Wu and Fang, 2011), and discrete equations are solved and programed by MATLAB. Paraffin wax is considered as PCM in the PT (Li et al., 2020c). It is worth noting that the validations of pool and PT models have been depicted in the study of Li et al. (2020b). The calculated average relative error of pool and PT models were 0.65% and 3.97%, respectively, and thus they were accurate and reliable.

## 6. Multi-objective optimization and decision-making methods

NSGA-II is utilized for performing the multi-objective optimal design. Two double-objective and one triple-objective optimal design are considered in this study. The design variables are $V_{pt}$ and $q_{ap}$. PT and ASHPs are core components of the heating system, which referred to the study of Li et al. (2018a), and thus the $V_{pt}$ and $q_{ap}$ that can reflect their characteristics in the system are also regarded as design variables in the multi-objective optimization problem. The objectives of two double-objective optimal design are minimizing $e_{tu}$ and $u_{tp}$, and minimizing $c_{lc}$ and $u_{tp}$. The objective of triple-objective optimal design is minimizing $e_{tu}, c_{lc}$, and $u_{tp}$. It should be noted that 15 years is considered as the period of a life cycle in this study. LP and TS are used for performing final decision-making based on the POSs. The detailed descriptions of NSGA-II, LP, and TS are depicted in the study of Li et al. (2020b).

## 7. Results and analysis

### *7.1. Training and validation of ANN model*

To obtain optimal ANN structure, different ANN structures with different hidden layers are compared. The number of neurons varies from one to ten when one hidden layer is utilized;

and it varies from one to six when two hidden layers are utilized. The ANN structure is considered as the optimal one when the mean square error is minimum. The results indicate that optimal ANN structure has two hidden layers. There are six and six neurons in first and second hidden layers, respectively. Mean square error of this ANN model is $1.66\times10^{-4}$. In this training model, the transient state of the ANN model when the epoch is 761 is selected as the final model. Fig. 6 shows the regressions of ANN: (a) training; (b) validation; (c) testing; and (d) all data. It is worth noting that before conducting the training of ANN model, the decimal places of output variables are unified. Hence, the ranges of both abscissa and ordinate are from 0 to 25. It can be seen that the predicted values match the target values very well. The values of $R$ for training, validation, testing, and all data are 1, 1, 0.99997, and 0.99999, respectively. Thus, the training ANN model is very accurate as the objective function.
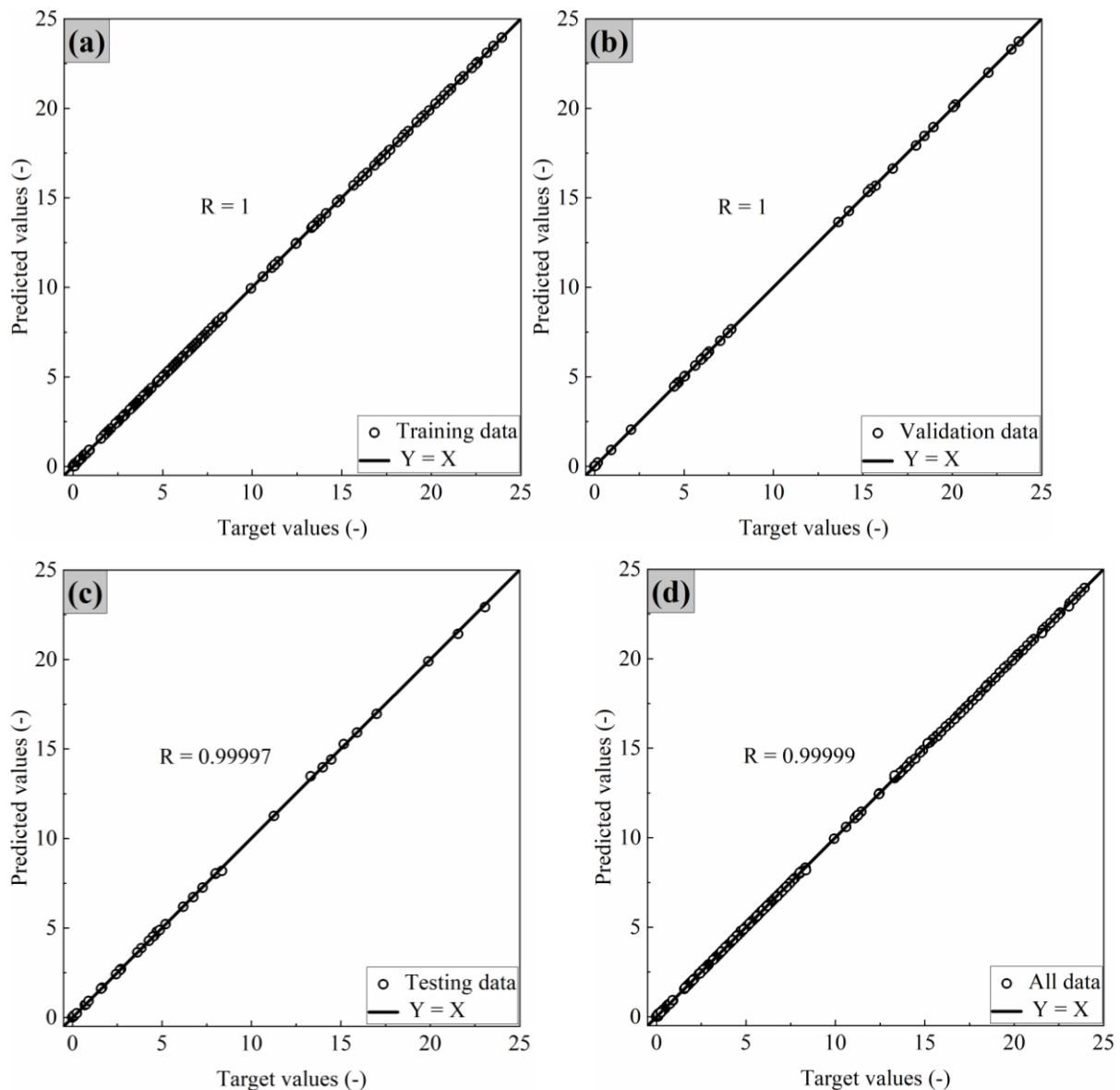
*7.2. Multi-objective optimization*

In multi-objective optimization, all combinations of optimization objectives (i.e. POSs) are optimal. Fig. 7 presents the POSs for the optimal design with two optimization objectives, (i.e. minimizing $e_{tu}$ and $u_{tp}$). The values of $e_{tu}$ reduce with the increase of $u_{tp}$. The solution with a lower $e_{tu}$ has a higher $u_{tp}$; while the solution with a higher $e_{tu}$ has a lower $u_{tp}$. The values of $e_{tu}$ are $1.51 \times 10^{10}$ kJ and $1.26 \times 10^{10}$ kJ when the values of $u_{tp}$ are 0% and 8%, respectively. Thus, the values of $e_{tu}$ can be decreased by 16.2% when the value of $u_{tp}$ increases from 0% to 8%.
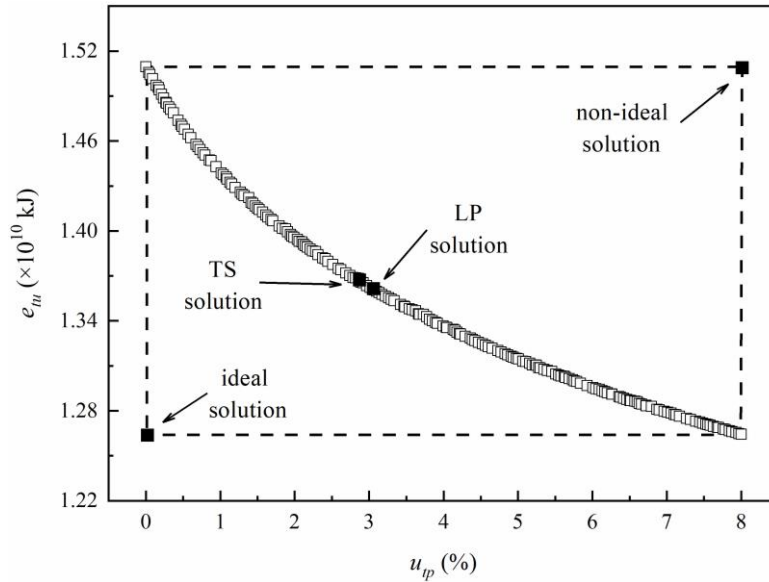


**Fig. 7.** POSs for double-objective optimization: minimizing $e_{tu}$ and $u_{tp}$.

Fig. 8 presents the POSs for the optimal design with two optimization objectives (i.e. minimizing $c_{lc}$ and $u_{tp}$). The values of $c_{lc}$ reduce with the increase of $u_{tp}$. The solution with a lower $c_{lc}$ has a higher $u_{tp}$; while the solution with a higher $c_{lc}$ has a lower $u_{tp}$. The values of $c_{lc}$ are €536,040 and €441,089 when the values of $u_{tp}$ are 0% and 8%, respectively. Thus, the value of $c_{lc}$ can be decreased by 17.7% when the value of $u_{tp}$ increases from 0% to 8%.
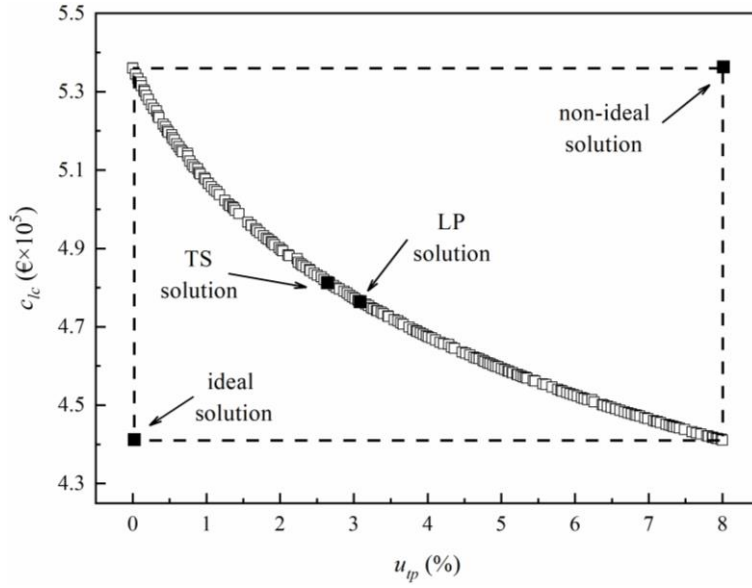
22

**Fig. 8.** POSs for double-objective optimization: minimizing $c_{lc}$ and $u_{tp}$.

Fig. 9 presents the POSs for the optimal design with triple optimization objectives (i.e. minimizing $e_{tu}$, $c_{lc}$, and $u_{tp}$). The values of $e_{tu}$ reduce with the increase of $u_{tp}$, and the values of $c_{lc}$ reduce with the increase of $u_{tp}$. The solution with a lower $e_{tu}$ and $c_{lc}$ has a higher $u_{tp}$; while the solution with a higher $e_{tu}$ and $c_{lc}$ has a lower $u_{tp}$. The values of $e_{tu}$ are $1.51 \times 10^{10}$ kJ and $1.26 \times 10^{10}$ kJ, and the values of $c_{lc}$ are €536,110 and €442,837, when the values of $u_{tp}$ are 0% and 8%, respectively. Thus, the values of $e_{tu}$ and $c_{lc}$ can be decreased by 16.2% and 17.4%, respectively, when the value of $u_{tp}$ increases from 0% to 8%.
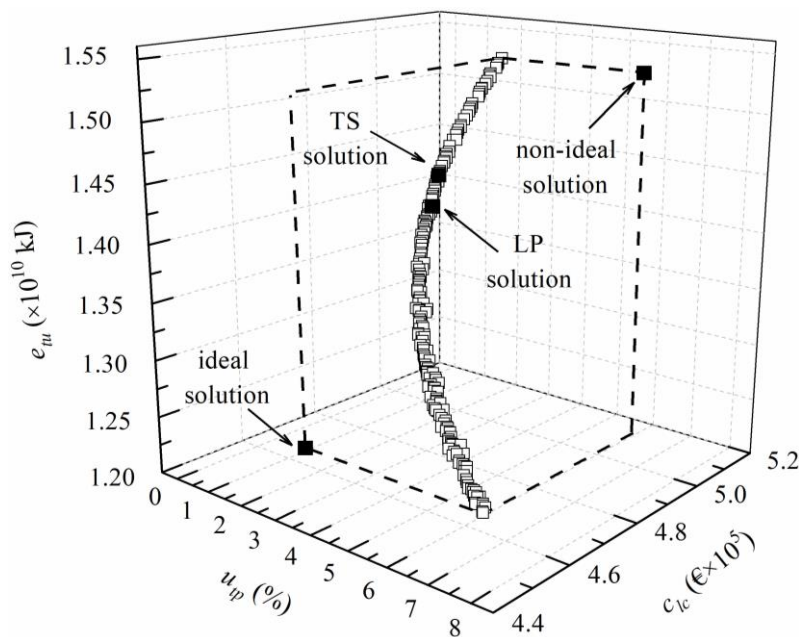
**Fig. 9.** POSs for triple-objective optimization: minimizing $e_{tu}$, $c_{lc}$, and $u_{tp}$.

### 7.3. Final decision-making

To conduct the final decision-making based on POSs by using LP and TS, non-ideal and ideal solutions are needed to be determined. As shown in Fig. 7, the non-ideal and ideal solutions for double-objective optimization of minimizing $e_{tu}$ and $u_{tp}$ are the solution with the values of $e_{tu}$ and $u_{tp}$ of $1.51 \times 10^{10}$ kJ and 8%, and the solution with the values of $e_{tu}$ and $u_{tp}$ of $1.26 \times 10^{10}$ kJ and 0%, respectively. As shown in Fig. 8, the non-ideal and ideal solutions for double-objective optimization of minimizing $c_{lc}$ and $u_{tp}$ are the solution with the values of $c_{lc}$ and $u_{tp}$ of €536,040 and 8%, and the solution with the values of $e_{tu}$ and $u_{tp}$ of €441,089 and 0%, respectively. As shown in Fig. 9, the non-ideal and ideal solutions for triple-objective optimization of minimizing $e_{tu}$, $c_{lc}$, and $u_{tp}$ are the solution with the values of $e_{tu}$, $c_{lc}$, and $u_{tp}$ of $1.51 \times 10^{10}$ kJ, €536,110, and 8%, and the solution with the values of $e_{tu}$, $c_{lc}$, and $u_{tp}$ of $1.26 \times 10^{10}$ kJ, €442,837, and 0%, respectively. Fig. 7, Fig. 8, and Fig. 9 also present the FOSs identified using LP and TS. Table 1 presents the FOSs after conducting decision-making for multi-objective optimal design.

**Table 1** FOSs after conducting decision-making

| Case | FOSs | $V_{pt}$ (m³) | $q_{ap}$ (kW) | $u_{tp}$ (%) | $e_{tu}$ ($\times 10^{10}$ kJ) | $c_{lc}$ (€$\times 10^5$) |
|---|---|---|---|---|---|---|
| 1 | LP-FOS for $e_{tu}$ and $u_{tp}$ | 71.7 | 264.2 | 3.01 | 1.36 | 4.78 |
| 2 | LP-FOS for $c_{lc}$ and $u_{tp}$ | 73.4 | 261.7 | 3.01 | 1.36 | 4.77 |
| 3 | LP-FOS for $e_{tu}$, $c_{lc}$, and $u_{tp}$ | 75.6 | 270.5 | 2.17 | 1.39 | 4.88 |
| 4 | TS-FOS for $e_{tu}$ and $u_{tp}$ | 71.8 | 264.7 | 2.97 | 1.36 | 4.79 |
| 5 | TS-FOS for $c_{lc}$ and $u_{tp}$ | 74.5 | 263.6 | 2.76 | 1.37 | 4.80 |
| 6 | TS-FOS for $e_{tu}$, $c_{lc}$, and $u_{tp}$ | 77.4 | 273.6 | 1.84 | 1.40 | 4.92 |

### 7.4. Performance analysis of FOSs

To analyze the system performance of FOSs shown in Table 1, the simulation of the system in winter in 2008 is conducted. Fig. 10 presents the 14-days (from February 3ʳᵈ, 2009 to February 16ᵗʰ, 2009) swimming pool water temperature variation in Case 1, in which the $V_{pt}$ and $q_{ap}$ are 71.7 m³ and 264.2 kW, respectively. It can be seen that during the preheating period, the water temperature increases because the ASHPs offer heat for the water. During the period between the preheating and open periods, in some days the water temperature decreases and in

other days the water temperature increases. During this period, there is no extra heat from PT and ASHPs that is offered into the pool water. The water temperature variations are caused by the weather conditions. If the heat gained is less than the heat loss of the water, the water temperature will decrease, and vice visa. During the open period, due to PID controller the water temperature is higher than 27°C, suggesting that thermal comfort requirement is met.
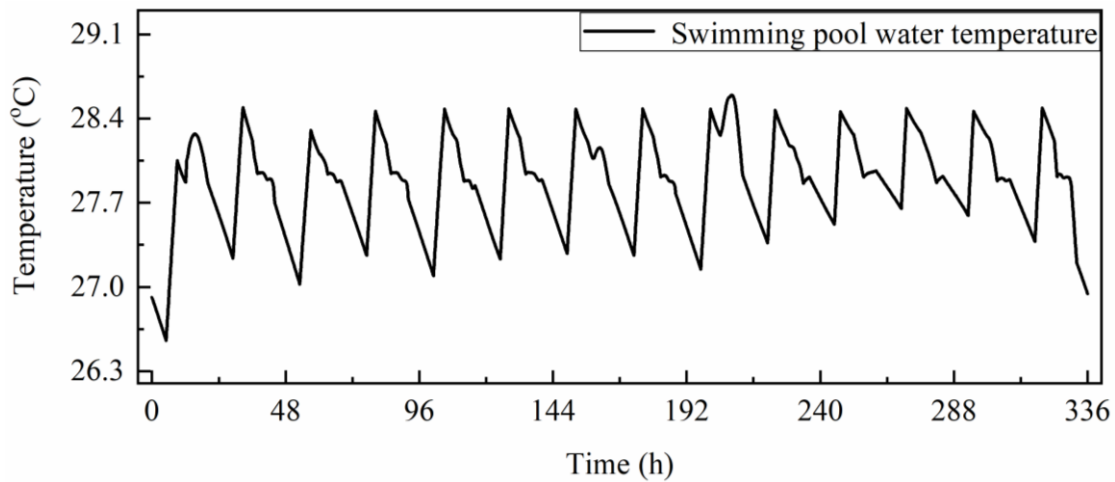


**Fig. 10.** 14-days (from February 3$^{rd}$, 2009 to February 16$^{th}$, 2009) temperature variation of the pool water in Case 1.

Fig. 11 presents the energy and operating cost saving ratio, and simple payback period of six different FOSs. Energy or operating cost saving ratio are equal to difference between electricity consumption or operating expense for proposed and conventional systems, dividing those of conventional systems. Simple payback period is equal to difference between operating expense of proposed and conventional systems, dividing initial expense of conventional systems. It is found that energy saving ratio of Case 1, 2, 3, 4, 5, and 6 are 76.2%, 76.1%, 75.8%, 76.1%, 76.1%, and 75.6%, respectively; operating cost saving ratio of Case 1, 2, 3, 4, 5, and 6 are 84.3%, 84.3%, 84.1%, 84.3%, 84.3%, and 84.0%, respectively; and simple payback period of Case 1, 2, 3, 4, 5, and 6 are 1.14, 1.13, 1.17, 1.14, 1.14, and 1.18 years, respectively. Hence, Case 1 has better energy performance than others because it has the highest energy saving ratio; and Case 2 has better economic performance than others because it has the highest operating cost saving ratio and shortest payback period.
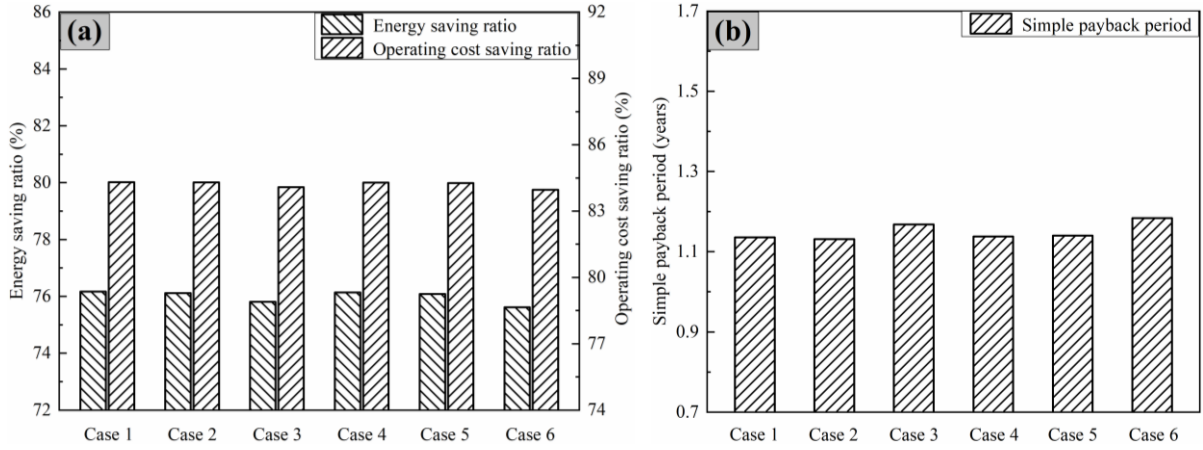
**Fig. 11.** (a) Energy and operating cost saving ratio; and (b) simple payback period in cases with different FOSs.

## 8. Conclusions and future prospects

An ANN-based multi-objective optimization approach was presented in this study. To well clarify this approach, a case study of a heating system for outdoor swimming pools was conducted. This heating system was utilized to extend the availability of a swimming pool in Hong Kong. NSGA-II was applied for conducting the multi-objective optimal design. The LP and TS were applied for conducting the decision-making to identify the FOSs from POSs. $V_{pt}$ and $q_{ap}$ were considered as design variables. The performance of the system with the FOSs was analyzed. The system energy and economic performance in these FOSs were considerable. The key conclusions were presented as follows:

- The ANN model was developed based on the constructed database, where 1,000 sets of data were obtained from the established simulation platform. Regression results of the developed ANN model showed that the values of R for training, validation, testing, and all data were 1, 1, 0.99997, and 0.99999, respectively. Thus, the ANN model was very reliable and accurate to be used for the multi-objective optimal design.

- Two double-objective optimizations in which the objectives were minimizing the $u_{tp}$ and $e_{tu}$, and minimizing the $u_{tp}$ and $c_{lc}$, respectively, were conducted. In the former double-objective optimization, optimal combinations of $V_{pt}$ and $q_{ap}$ in the LP-FOS and TS-FOS were 71.7 m³ and 264.2 kW, and 71.8 m³ and 264.7 kW, respectively. The corresponding $u_{tp}$, $e_{tu}$, and $c_{lc}$ in the LP-FOS and TS-FOS were 3.01%, 1.36×10¹⁰ kJ, and €477,965, and 2.97%, 1.36×10¹⁰ kJ, and €478,559, respectively. In the latter double-objective optimization, optimal combinations of $V_{pt}$ and $q_{ap}$ in the LP-FOS and TS-FOS were

26

73.4 m$^3$ and 261.7 kW, and 74.5 m$^3$ and 263.6 kW, respectively. The corresponding $u_{tp}$, $e_{tu}$, and $c_{lc}$ in the LP-FOS and TS-FOS were 3.01%, 1.36×10$^{10}$ kJ, and €477,206, and 2.76%, 1.37×10$^{10}$ kJ, and €480,038, respectively.

- Triple-objective optimization in which the objective was minimizing the $u_{tp}$, $c_{lc}$, and $e_{tu}$, was conducted. The optimal combinations of the $V_{pt}$ and $q_{ap}$ in the LP-FOS and TS-FOS were 75.6 m$^3$ and 270.5 kW, and 77.4 m$^3$ and 273.6 kW, respectively. The corresponding $u_{tp}$, $e_{tu}$, and $c_{lc}$ in the LP-FOS and TS-FOS were 2.17%, 1.39×10$^{10}$ kJ, and €487,812, and 1.84%, 1.40×10$^{10}$ kJ, and €492,491, respectively.

Hence, the results indicated that proposed approach could effectively guide optimization for the heating system. This method used data generated by simulation platform to develop the ANN model, which well reflected the physical characteristics of the system. This made the results of multi-objective optimal design more meaningful. Therefore, it provided a useful and instructive guideline of optimal design for other BSs. However, there were some works that could be conducted in the future, shown below:

- Evaporative heat transfer coefficient calculated by empirical formula, and pressure difference between water-surface saturated and ambient partial vapor were used for calculating the evaporative heat loss during the open period. In fact, the number and activities of swimmers might affect the evaporative heat loss. The evaporative heat loss might be expressed as the functions of the number and activities of swimmers. The heat generated from the bodies of swimmers might affect the water evaporation and heat gained by water, which might affect the temperature variation of the pool water. These factors should be considered in future works.

- The temperature of the pool water in different places was assumed to be equal. However, in real conditions it was different. The shading area of the pool might be different in a sunny day, and thus the heat obtained from the sun might be different in different period of the day. The effect of different heat obtained from the sun on the temperature variation of the pool water should be considered in future works.

- The "trainlm" was selected as the training function to develop the ANN model. Other training functions (e.g. "trainrp" and "trainbfg") should be considered, and the performance of the ANN models using different training functions should be compared in future works.

**References**

Abd Alla, S., Bianco, V., Tagliafico, L.A., Scarpa, F., 2020. An innovative approach to local solar energy planning in Riva Trigoso, Italy. Journal of Building Engineering 27.

Bejan, A., 2015. Sustainability: The Water and Energy Problem, and the Natural Design Solution. European Review 23(4), 481-488.

Buonomano, A., De Luca, G., Figaj, R.D., Vanoli, L., 2015. Dynamic simulation and thermo-economic analysis of a PhotoVoltaic/Thermal collector heating system for an indoor–outdoor swimming pool. Energy Conversion and Management 99, 176-192.

Chan, W.W., Lam, J.C., 2003. Energy-saving supporting tourism sustainability: A case study of hotel swimming pool heat pump. Journal of Sustainable Tourism 11(1), 74-83.

Chen, Q., Ja, M.K., Li, Y., Chua, K.J., 2018. Energy, economic and environmental (3E) analysis and multi-objective optimization of a spray-assisted low-temperature desalination system. Energy 151, 387-401.

Dang, A., 1986. A parametric study of swimming pool heating—I. Energy Conversion and management 26(1), 27-31.

Deb, K., Pratap, A., Agarwal, S., Meyarivan, T., 2002. A fast and elitist multiobjective genetic algorithm: NSGA-II. IEEE transactions on evolutionary computation 6(2), 182-197.

Deng, Z., Chen, Q., 2018. Artificial neural network models using thermal sensations and occupants' behavior for predicting thermal comfort. Energy and Buildings 174, 587-602.

Ding, Y., Zhang, Q., Yuan, T., Yang, F., 2018. Effect of input variables on cooling load prediction accuracy of an office building. Applied Thermal Engineering 128, 225-234.

Du, Y., Blocken, B., Pirker, S., 2020. A novel approach to simulate pollutant dispersion in the built environment: Transport-based recurrence CFD. Building and Environment 170.

Du, Y., Mak, C.M., Ai, Z., 2018. Modelling of pedestrian level wind environment on a high-quality mesh: A case study for the HKPolyU campus. Environmental Modelling & Software 103, 105-119.

Etghani, M.M., Shojaeefard, M.H., Khalkhali, A., Akbari, M., 2013. A hybrid method of

28

modified NSGA-II and TOPSIS to optimize performance and emissions of a diesel engine using biodiesel. Applied Thermal Engineering 59(1-2), 309-315.

Evola, G., Fichera, A., Gagliano, A., Marletta, L., Nocera, F., Pagano, A., Palermo, V., 2016. Application of a Mapping tool to Plan Energy Saving at a Neighborhood Scale. Energy Procedia 101, 137-144.

Fichera, A., Frasca, M., Palermo, V., Volpe, R., 2018. An optimization tool for the assessment of urban energy scenarios. Energy 156, 418-429.

Gang, W., Wang, S., Augenbroe, G., Xiao, F., 2016. Robust optimal design of district cooling systems and the impacts of uncertainty and reliability. Energy and Buildings 122, 11-22.

Incropera, F.P., Lavine, A.S., Bergman, T.L., DeWitt, D.P., 2007. Fundamentals of heat and mass transfer. Wiley.

Kennedy, S., Johnson, C.K., 2016. Perfecting China, Inc.: China's 13th Five-Year Plan. Rowman & Littlefield.

Klein, S., Beckman, A., Mitchell, W., Duffie, A., 2011. TRNSYS 17-A TRansient SYstems Simulation program. Solar Energy Laboratory, University of Wisconsin, Madison.

Lam, J.C., Chan, W.W., 2001. Life cycle energy cost analysis of heat pump application for hotel swimming pools. Energy Conversion and Management 42(11), 1299-1306.

Li, X., Peng, J., Li, N., Wu, Y., Fang, Y., Li, T., Wang, M., Wang, C., 2019. Optimal design of photovoltaic shading systems for multi-story buildings. Journal of Cleaner Production 220, 1024-1038.

Li, Y., Ding, Z., Du, Y., 2020a. Techno-economic optimization of open-air swimming pool heating system with PCM storage tank for winter applications. Renewable Energy 150, 878-890.

Li, Y., Ding, Z., Shakerin, M., Zhang, N., 2020b. A multi-objective optimal design method for thermal energy storage systems with PCM: A case study for outdoor swimming pool heating application. Journal of Energy Storage 29.

Li, Y., Huang, G., Wu, H., Xu, T., 2018a. Feasibility study of a PCM storage tank integrated heating system for outdoor swimming pools during the winter season. Applied Thermal Engineering 134, 490-500.

Li, Y., Huang, G., Xu, T., Liu, X., Wu, H., 2018b. Optimal design of PCM thermal storage tank and its application for winter available open-air swimming pool. Applied Energy 209, 224-235.

Li, Y., Zhang, N., Ding, Z., 2020c. Investigation on the energy performance of using air-source heat pump to charge PCM storage tank. Journal of Energy Storage 28.

Liu, C., Xu, W., Li, A., Sun, D., Huo, H., 2019. Energy balance evaluation and optimization of photovoltaic systems for zero energy residential buildings in different climate zones of China. Journal of Cleaner Production 235, 1202-1215.

Mavromatidis, L., 2018. Coupling architectural synthesis to applied thermal engineering, constructal thermodynamics and fractal analysis: An original pedagogic method to incorporate "sustainability" into architectural education during the initial conceptual stages. Sustainable Cities and Society 39, 689-707.

Mavromatidis, L., 2019. Constructal Macroscale Thermodynamic Model of Spherical Urban Greenhouse Form with Double Thermal Envelope within Heat Currents. Sustainability 11(14).

Mavromatidis, L.E., 2015. A review on hybrid optimization algorithms to coalesce computational morphogenesis with interactive energy consumption forecasting. Energy and Buildings 106, 192-202.

Mavromatidis, L.E., 2016. Study of coupled transient radiation-natural convection heat transfer across rectangular cavities in the vicinity of low emissivity thin films for innovative building envelope applications. Energy and Buildings 120, 114-134.

Mousia, A., Dimoudi, A., 2015. Energy performance of open air swimming pools in Greece. Energy and Buildings 90, 166-172.

Moussa, R.R., Mahmoud, A.H., Hatem, T.M., 2020. A digital tool for integrating renewable energy devices within landscape elements: Energy-scape online application. Journal of Cleaner Production 254.

Nasruddin, Sholahudin, Satrio, P., Mahlia, T.M.I., Giannetti, N., Saito, K., 2019. Optimization of HVAC system energy consumption in a building using artificial neural network and multi-objective genetic algorithm. Sustainable Energy Technologies and Assessments 35, 48-57.

Ruiz, E., Martínez, P.J., 2010. Analysis of an open-air swimming pool solar heating system by using an experimentally validated TRNSYS model. Solar Energy 84(1), 116-123.

Schwarz, M., Nakhle, C., Knoeri, C., 2020. Innovative designs of building energy codes for building decarbonization and their implementation challenges. Journal of Cleaner Production 248.

Sinha, A., Shahbaz, M., Sengupta, T., 2018. Renewable energy policies and contradictions in causality: A case of Next 11 countries. Journal of Cleaner Production 197, 73-84.

Somwanshi, A., Tiwari, A.K., Sodha, M.S., 2013. Feasibility of earth heat storage for all weather conditioning of open swimming pool water. Energy Conversion and Management 68, 89-95.

Srinivasan, V., Shocker, A.D., 1973. Linear programming techniques for multidimensional analysis of preferences. Psychometrika 38(3), 337-369.

Tang, Z., Zhang, Z., 2019. The multi-objective optimization of combustion system operations based on deep data-driven models. Energy 182, 37-47.

TrialandErrorMethod, 2020. Trial and Error Method. https://www.smlease.com/entries/automation/what-is-pid-proportional-integral-derivative-control/.

Turhan, C., Kazanasmaz, T., Uygun, I.E., Ekmen, K.E., Akkurt, G.G., 2014. Comparative study of a building energy performance software (KEP-IYTE-ESS) and ANN-based building heat load estimation. Energy and Buildings 85, 115-125.

Volpe, R., Frasca, M., Fichera, A., Fortuna, L., 2016. The role of autonomous energy production systems in urban energy networks. Journal of Complex Networks.

von Grabe, J., 2016. Potential of artificial neural networks to predict thermal sensation votes. Applied Energy 161, 412-424.

Woolley, J., Harrington, C., Modera, M., 2011. Swimming pools as heat sinks for air conditioners: Model design and experimental validation for natural thermal behavior of the pool. Building and Environment 46(1), 187-195.

Wu, S., Fang, G., 2011. Dynamic performances of solar heat storage system with packed bed using myristic acid as phase change material. Energy and Buildings 43(5), 1091-1096.

Xu, T., Li, Y., Chen, J., Liu, J., 2017. Preparation and thermal energy storage properties of LiNO $_3$ -KCl-NaNO $_3$ /expanded graphite composite phase change material. Solar Energy

Materials and Solar Cells 169, 215-221.

Xu, T., Li, Y., Chen, J., Wu, H., Zhou, X., Zhang, Z., 2018. Improving thermal management of electronic apparatus with paraffin (PA)/expanded graphite (EG)/graphene (GN) composite material. Applied Thermal Engineering 140, 13-22.

Yan, Y., Zhang, H., Long, Y., Wang, Y., Liang, Y., Song, X., Yu, J.J.Q., 2019. Multi-objective design optimization of combined cooling, heating and power system for cruise ship application. Journal of Cleaner Production 233, 264-279.

Zhou, Y., Zheng, S., 2020. Machine learning-based multi-objective optimisation of an aerogel glazing system using NSGA-II—study of modelling and application in the subtropical climate Hong Kong. Journal of Cleaner Production 253.

1
2
3
4
5
6
7
8
9
10
11
12
13
14
15
16
17
18
19
20
21
22
23
24
25
26
27
28
29
30
31
32
33
34
35
36
37
38
39
40
41
42
43
44
45
46
47
48
49
50
51
52
53
54
55
56
57
58
59
60
61
62
63
64
65